

# Experimental study of transient nitric oxide, smoke, and combustion noise emissions during acceleration of an automotive turbocharged diesel engine

C D Rakopoulos\*, A M Dimaratos, and E G Giakoumis

Internal Combustion Engines Laboratory, Department of Thermal Engineering, School of Mechanical Engineering, National Technical University of Athens, Athens, Greece

*The manuscript was received on 19 January 2010 and was accepted after revision for publication on 30 July 2010.*

DOI: 10.1243/09544070JAUTO1493

**Abstract:** The control of transient emissions from turbocharged diesel engines is an important objective for automotive manufacturers, since newly produced engines must meet the stringent criteria concerning exhaust emissions levels as dictated by the legislated Transient Cycles Certification. In the current study, experimental tests are conducted on an automotive, turbocharged diesel engine in order to investigate the formation mechanism of nitric oxide, smoke, and combustion noise emissions under various acceleration schedules experienced during daily driving conditions. To this aim, a fully instrumented test bed was set up in order to capture the development of key engine and turbocharger variables during the transient events. Analytical diagrams are provided to explain the behaviour of emissions development in conjunction with turbocharger and governor/fuel pump response. Turbocharger lag was found to be the main cause for the emission spikes during all test cases examined, with the engine calibration playing a vital role. The analysis was extended with a quasi-steady approximation of transient emissions using steady-state maps, in order to highlight the effect of dynamic engine operation on pollutants and combustion noise emissions.

**Keywords:** transient emissions, nitric oxide, smoke, combustion noise, acceleration, automotive diesel engine

## 1 INTRODUCTION

The turbocharged diesel engine is currently the preferred powertrain system in medium and medium-large unit applications (trucks, land traction, ship propulsion, electricity generation, etc.). Moreover, it continuously increases its share in the highly competitive automotive market, having already ensured a market share comparable to the one of the gasoline engine [1]. The most attractive feature of the diesel engine is its very good fuel efficiency, which can surpass a value of 40 per cent in vehicular applications and even 50 per cent in large, two-stroke units

used for marine propulsion or electricity generation. Consequently, diesel-engined vehicles achieve much lower fuel consumption and reduced carbon dioxide emissions than their similarly rated spark ignition counterparts over the entire operating range and for their whole lifetime.

Traditionally, the study of diesel engine operation has focused on the steady-state performance, with much less attention paid to their transient operation. However, the majority of daily driving schedules involve transient conditions with only a very small portion of a vehicle's operating pattern being truly steady state, e.g. when cruising on a motorway. Thus, the experimental and modelling investigation of diesel engine transient operation has turned out to be an important objective for engine manufacturers, intensified by the fact of significant deviations experienced when comparing instantaneous transient emissions with their quasi-steady counterparts [2–6]. Acknowl-

\*Corresponding author: Internal Combustion Engines Laboratory, Department of Thermal Engineering, School of Mechanical Engineering, National Technical University of Athens, 9 Heroon Polytechniou St, Zografou Campus, 15780, Athens, Greece. email: cdrakops@central.ntua.gr

edging the previously mentioned findings, various legislative directives in the European Union, Japan, and the US, have drawn the attention of manufacturers and researchers from all over the world to the transient operation of diesel engines in the form of Transient Cycles Certification for new vehicles [7–9].

The fundamental aspect of transient conditions lies in its operating discrepancies compared to the respective steady-state ones (i.e. operation at the same engine rotational speed and fuel pump rack position). While during steady-state operation engine speed and fuelling and so, consequently, all the other engine and turbocharger properties remain practically constant, under transient conditions both the engine speed and fuel supply change continuously. Consequently, the available exhaust gas energy varies, affecting turbine enthalpy drop and, through the turbocharger shaft torque balance, the boost pressure and the air supply to the engine cylinders are influenced. However, due to various dynamic, thermal, and fluid delays in the system (mainly originating in the turbocharger moment of inertia – turbocharger lag), combustion air supply is delayed compared to fuelling, thus adversely affecting torque build-up and emissions [2].

It is the turbocharger's mass moment of inertia that proves to be the most significant delay decisively influencing engine performance and emissions. The importance of various other transient discrepancies compared to steady-state operation, can be evaluated through a qualitative order-of-magnitude analysis, a technique widely applied in unsteady computations in turbomachinery [10, 11]. Thus, after the turbocharger inertia, it is the cylinder and the exhaust manifold wall temperature, the flow inertia in filling the manifolds, and the in-cylinder trapped exhaust gas (as a result of the high back pressure combined with low boost pressure) that play a vital role in the engine's transient performance, contributing to the emission peaks experienced under dynamic conditions.

However, this vital issue of emissions overshoot during transients has not been investigated adequately but rather segmentally, owing to the difficulties that both the modelling and experimental approaches encounter. For the simulation procedure, a multi-zone (or at least a two-zone) combustion model is needed for the prediction of exhaust emissions. Such models require careful estimation of a large number of calibrated constants for each sub-model developed, which forms a tremendous task. Furthermore, a plethora of detailed engine data (turbocharger maps, governor/fuel pump curves, valve train and piston assembly characteristics etc.), which are usually unavailable, are required for a successful simulation of

transient processes. On the other hand, the experimental investigation of transient emissions demands highly complicated, sophisticated, and costly experimental equipment, such as a fully automated test bed with electronically controlled dynamometer and fast response exhaust gas analysers.

As a result, relatively few experimental works have been conducted so far (see, for example, [3, 12–16]), while simulation studies are even more scarce [17–20] with sometimes questionable results. In particular, as regards the transient numerical simulations, two-zone and multi-zone combustion models have been occasionally developed in the past, often with only partial experimental validation mainly by relatively simple and 'slow' response analysing techniques (signal reconstruction, sampling method), a fact that has limited the reliability of their results. Unsurprisingly, alternative modelling approaches have been proposed for predicting (diesel engine) transient emissions, e.g. based on steady-state mapping and applying correction factors to account for transient discrepancies [21–23], or by reconstructing the measured signal recorded by conventional slow response analysers [24, 25].

The aim of this study is to expand on the experimental investigation of transient vehicular diesel engine operation, and shed more light on the relevant complex phenomena and underlying mechanisms of emissions formation with respect to engine performance. To this aim, an extended set of experimental tests has been conducted on a medium-duty, turbocharged and after-cooled, direct injection, automotive/truck diesel engine using ultra-fast response analysers, in order to capture the instantaneous emissions during each transient event. The investigation concerns cases of transient operation experienced in daily vehicle driving, i.e. acceleration with simultaneous load increase as well as complex transients such as load (resistance) increase followed by vehicle acceleration, e.g. gear change during climbing up a hill.

The experimental investigation carried out here focused on the measurement of the two most significant diesel engine pollutants, i.e. nitric oxide (NO) and smoke, but it was also extended to another important (and often neglected) emission, namely combustion noise. Diesel engine noise radiation has received increasing attention in recent years [26–28], since it is associated with passengers' and pedestrians' comfort levels. The primary sources of noise generation in a diesel engine are gas flow in the exhaust system (usually limited using mufflers (silencers) along the exhaust pipe), mechanical processes (e.g. valve train, gears), and combustion. The latter (otherwise

stated as 'combustion roughness') prevails over other, mechanically originated, noise radiation [2], and this is why only this source of noise was studied in the current work. By including this measurement in the investigation, it was made possible to derive some useful conclusions regarding the underlying common mechanisms between the three examined emissions.

## 2 DESCRIPTION OF THE EXPERIMENTAL INSTALLATION

A general layout of the test bed installation, the instrumentation used, and the data acquisition system is illustrated in Fig. 1. A brief description of the individual components will be given in the following sections.

### 2.1 Engine under study

The engine used in this study was a Mercedes-Benz OM 366 LA, turbocharged and after-cooled, direct injection diesel engine, following the Euro II emissions standard. It is widely used to power mini-buses and small/medium trucks. Its basic technical data are given in Table 1. Two notable features of the engine are, on the one hand its retarded fuel injection timing in order to achieve low NO emissions and, on the other hand, the fuel-limiter (cut-off) function in order to limit the exhaust smoke level during demanding conditions such as transients or low-speed, high-load steady-state operations. The engine was coupled to a hydraulic dynamometer, which allowed a good simulation of a vehicle's acceleration as will be explained later in the text.

### 2.2 Emissions measurement

#### 2.2.1 NO measurement

For the continuous measurement of NO emission, the ultra-fast response analyser CLD500 by Combustion Ltd [29] was employed. This is a chemilumi-

nescent detector used for measuring NO and NO<sub>x</sub> (in the latter case incorporating a NO<sub>2</sub> to NO converter) concentration in the exhaust gas with a 90–10 per cent response time of approximately 2 ms for NO and 10 ms for NO<sub>x</sub> [30]. These very short response times were achieved by locating the detectors in remote sample heads, which were positioned very close to the sample point in the engine, and by conveying the sample gas to the detectors under the influence of a vacuum through narrow heated capillaries. The linearity of the analyser is less than  $\pm 1$  per cent FSO (full scale output) and its drift less than  $\pm 1$  per cent FSO per hour.

The CLD500 equipment has two remote sampling heads controlled by a mains control unit and it is capable of simultaneous sampling at two different locations. For the current study, the two sampling (head) positions are shown in Fig. 1. The first head was located exactly after the exhaust valve of cylinder 1 (this is the same cylinder from which the indicator diagrams were measured) capturing the individual cylinder's NO concentration, and the second head was located downstream of the turbocharger capturing total NO emission concentration. Both heads were used during steady-state experiments, whereas during transient testing only the second sampling head was used owing to data acquisition card limitations.

#### 2.2.2 Opacity measurement

The exhaust gas (smoke) opacity was measured continuously with an AVL 439 partial flow opacimeter. This is a device particularly suitable for dynamic testing measurements with the exhaust gas sample flowing continuously through the opacimeter with a constant flowrate. The response time of the opacimeter is less than 0.1 s and its accuracy is 0.1 per cent opacity. The opacity of the sample is determined from the measurement of the attenuation of visible light by the smoke in the exhaust gas sample located between the (light

**Table 1** Engine and turbocharger specifications

Engine model and type	'Mercedes Benz', OM 366 LA, 6 cylinder, in-line, 4 stroke, compression ignition, direct injection, water-cooled, turbocharged, after-cooled, with bowl-in-piston
Emissions standard	Euro II
Speed range	800–2600 rpm
Maximum power	177 kW at 2600 rpm
Maximum torque	840 Nm at 1250–1500 rpm
Engine total displacement	5958 cm <sup>3</sup>
Bore/stroke	97.5 mm/133 mm
Compression ratio	18:1
Fuel pump	'Bosch' PE-S series, in-line, 6 cylinder with fuel limiter
Static injection timing	5 $\pm$ 1° crank angle before top dead centre (at full load)
Turbocharger model	'Garrett' TBP 418-1 with internal waste-gate
Aftercooler	Air-to-air

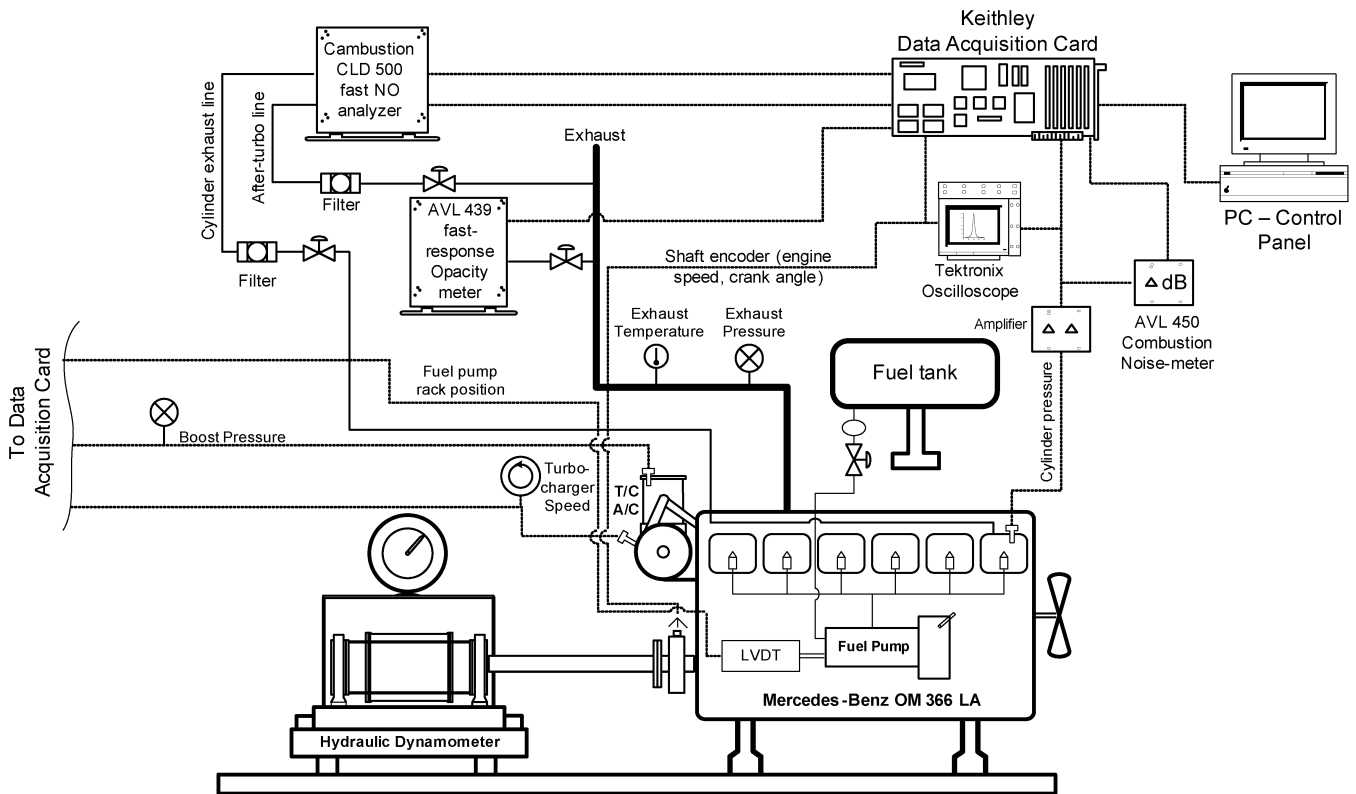


**Fig. 1** Schematic arrangement of the test bed installation, instrumentation, and data acquisition system

source and the detector unit [31]. The opacimeter outputs the measurement either in terms of opacity values  $N$  (0–100 per cent), as in the case of the present study, or absorption coefficient values  $k$  ( $0\text{--}10\text{ m}^{-1}$ ). Its technical characteristics comply with legal requirements such as ECE R24, SAE J 1667, and the ELR Test Cycle, with the respective filter algorithms pre-programmed into the opacimeter. In this study, no filter algorithm was applied ('raw' signal) in order to capture successfully all the smoke emission peaks. The location of sampling and return lines, as can be seen in Fig. 1, was downstream of the turbocharger.

### 2.2.3 Combustion noise measurement

The origin of combustion noise in a diesel engine (the characteristic diesel combustion 'knock') originates in the high rate of cylinder pressure rise  $dp/d\phi$ , mainly during the premixed phase of combustion after the ignition delay. Combustion noise measurement was achieved using the AVL 450 Combustion Noise Meter. Its operating principle is based on the analysis of the cylinder pressure diagrams in the frequency domain, and applying a series of filters to it [32], such as U-filter, selectable low-pass filters, and A-filter. The produced output signal was further

processed by root mean square conversion to logarithmic d.c. values. The total error of the meter is less than  $\pm 1$  dB. In the present work, the combustion noise meter was placed after the cylinder pressure signal amplifier, as shown in Fig. 1, and was operated without any low-pass filter.

### 2.3 Measurement of engine and turbocharger operating parameters

The engine and turbocharger operating parameters measured and recorded continuously were the engine speed, cylinder pressure, fuel pump rack position, boost pressure, and turbocharger speed. The location of each measuring device on the experimental test bed installation is shown in Fig. 1. Table 2 provides a brief list of the various measuring devices; a more detailed description can be found in [16]. A custom made 'stop' with various adjustable positions, each one corresponding to a specific engine speed, was fitted on the (accelerator) pedal in order to ensure a constant pedal position at the end of each acceleration test as well as repeatability of the accelerations.

Exhaust pressures and temperatures at various locations were also measured during steady-state conditions with conventional analogue devices. Addi-

**Table 2** Measuring devices for engine and turbocharger operating parameters

Parameter	Measuring device
Engine speed	'Kistler' shaft encoder
Cylinder pressure	'Kistler' miniature piezoelectric transducer, combined with 'Kistler' charge amplifier
Fuel pump rack position	Linear variable differential transducer (LVDT)
Boost pressure	'Wika' pressure transmitter
Turbocharger speed	'Garrett' turbo speed sensor (including gauge)

tionally, fuel consumption measurements were undertaken during steady-state operation with the use of a gravimetric fuel tank.

### 2.4 Data acquisition and processing system

All the previously mentioned signals from the measuring devices and instruments were fed to the input of the data acquisition module, which was a Keithley KUSB 3102 ADC card connected to a Pentium Dual Core PC via a USB interface. The specific card has a maximum sampling rate of 100 ksamples/s, with a 12-bit resolution for its eight differential analogue inputs. For the present study and during transient measurements, the inputs were used as follows. 1: engine speed; 2: fuel pump rack position; 3: cylinder pressure; 4: turbocharger speed; 5: boost pressure; 6: combustion noise; 7: (smoke) opacity; and 8: NO emission. Following the storage of the recorded measurements into files, the data were processed using an in-house developed computer code.

## 3 POST-PROCESSING OF THE EXPERIMENTAL DATA

### 3.1 Calculation of the brake mean effective pressure, the brake specific fuel consumption, and the brake thermal efficiency

For the mapping of engine performance and emissions during steady-state operating conditions (needed for the quasi-steady approximation in section 6), three basic parameters were calculated, namely the brake mean effective pressure (*bmep*), the brake specific fuel consumption (*bsfc*), and the brake thermal efficiency (*bte*). The first one can be calculated by

$$bmep = \frac{4\pi M_t}{V_H} \times 10^{-5} \quad (1)$$

where  $M_t$  is the engine brake torque as indicated on

the dynamometer and  $V_H = z(\pi D^2/4)s$  is the total engine displacement volume, with  $z$  being the number of cylinders, and  $D$ ,  $s$  the cylinder bore and piston stroke, respectively. Then, engine brake power can be calculated as

$$P = M_t \times \frac{2\pi n}{60} \quad (2)$$

where  $n$  is the engine rotational speed. After that, *bsfc* and *bte* can be found by

$$bsfc = \frac{V_{fc} \times \rho_f}{P} \times 3.6 \times 10^9$$

$$bte = \frac{P}{V_{fc} \times \rho_f \times \Theta} \quad (3)$$

where  $V_{fc}$  is the volumetric fuel consumption rate,  $\rho_f$  is the fuel density, and  $\Theta$  the lower calorific value of the fuel.

### 3.2 NO measurement processing

The measured concentration values of NO during transient testing were converted into mass values (mg/cycle) using the following relationship

$$m_{NO} = \frac{C_{NO}}{1000} \times \frac{MW_{NO}}{MW_{eg}} \times m_{eg} \quad (4)$$

where  $C_{NO}$  is the measured NO concentration,  $MW_{NO}$  and  $MW_{eg}$  are the NO and exhaust gas molecular weights, respectively, and  $m_{eg}$  is the exhaust gas mass per engine cycle. The latter includes both air and fuel mass. The in-cylinder trapped air mass was calculated by applying the perfect gas equation of state at the inlet valve closure, using the measured values of boost pressure and temperature. For the calculation of total air mass, an estimation of the trapping efficiency (0.85–0.90) was needed. On the other hand, the fuel mass supply during each cycle of the transient event was found using the steady-state fuel pump operating curves for the instantaneous measured rack position.

### 3.3 Opacity measurement processing

In order to calculate the total soot mass emitted during the tests, the following procedure was applied [33]. Initially, the absorption coefficient was calculated from the opacity value

$$k = \frac{-\ln[1 - (N/100)]}{L} \quad (5)$$

and then soot density (*SD*) was derived by

$$SD = \frac{10^6 \times 1000 \times k}{S_p} \quad (6)$$

where *S<sub>p</sub>* is a constant depending on the temperature of the sample inside the opacimeter [33].

The soot density could be converted into the soot mass concentration (*SMC*) in the exhaust gas by dividing it with the exhaust gas density inside the measuring chamber of the opacimeter

$$SMC = \frac{SD}{\rho_{eg}} = SD / \left[ (p_{eg} \times MW_{eg}) / (R_m \times T) \right] \quad (7)$$

where *p<sub>eg</sub>* is the sample pressure in the opacimeter (usually equal to atmospheric pressure). Finally, soot mass could be found by multiplying *SMC* with the exhaust gas mass

$$m_{soot} = SMC \times m_{eg} \quad (8)$$

For the case of the AVL opacimeter 439 used in this study, the optical path length *L* is 43 cm and the sample temperature *T* is 373 K.

#### 4 EXPERIMENTAL PROCEDURE

The first task of the test bed installation was the investigation of the steady-state performance and emissions characteristics of the examined engine. To this aim, an extended series of steady-state trials were conducted, as detailed in Table 3, covering the whole engine speed and load operating range. Between two consecutive measurements, a time interval was allowed in order for the engine to stabilize at the new conditions. The criterion used here was the stabilization of the exhaust gas temperature.

The main task of the experimental procedure was to study the engine transient response and emissions development during accelerations. Since the engine was coupled to a hydraulic dynamometer, during all acceleration cases the brake load (resistance) increased accordingly. This is actually the case when a vehicle accelerates in real-world driving; the increase in engine/vehicle speed results in an increase of both tyre rolling and aerodynamic resistance. In all test

**Table 3** Tabulation of test conditions for steady-state tests

Engine speed (rpm)	1000, 1200, 1400, 1600, 1800, 2000, 2200
Load (%)	10, 30, 50, 70, 80 (or 90)

cases, the engine was allowed to stabilize at the initial steady-state condition and then the pedal was pushed to the end of the adjustable custom made ‘stop’ to accelerate the engine.

The acceleration tests were performed for various combinations of initial engine rotational speeds and loads, mimicking vehicle real acceleration under different (vehicle) speed and gear; the details are given in Table 4. Also, Fig. 2 provides an illustration of the initial and final conditions of each test in a speed–load graph. A more detailed description of each test is given in the corresponding results section. It should be noted that a good repeatability of the results was confirmed, with the emission values being reproducible, after repetition of some tests under the same conditions.

### 5 RESULTS AND DISCUSSION

#### 5.1 Steady-state results

Figures 3 and 4 illustrate the results of the performed steady-state tests. Only the results from four engine speeds are given here in order for the diagrams to be clear and easily understood. These figures build up the

**Table 4** Tabulation of test conditions for acceleration tests

Test	Initial conditions		Final conditions	
	Speed (rpm)	Load (%)	Speed (rpm)	Load (%)
1	1016	10	1880	15
2	1420	30	1845	52
3	1825	30	2022	77
4	1035	10	1670	12

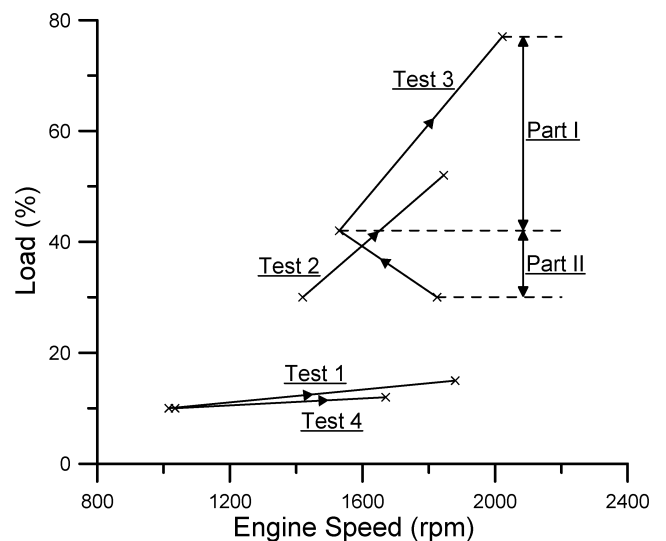


**Fig. 2** Initial–final conditions of each transient test

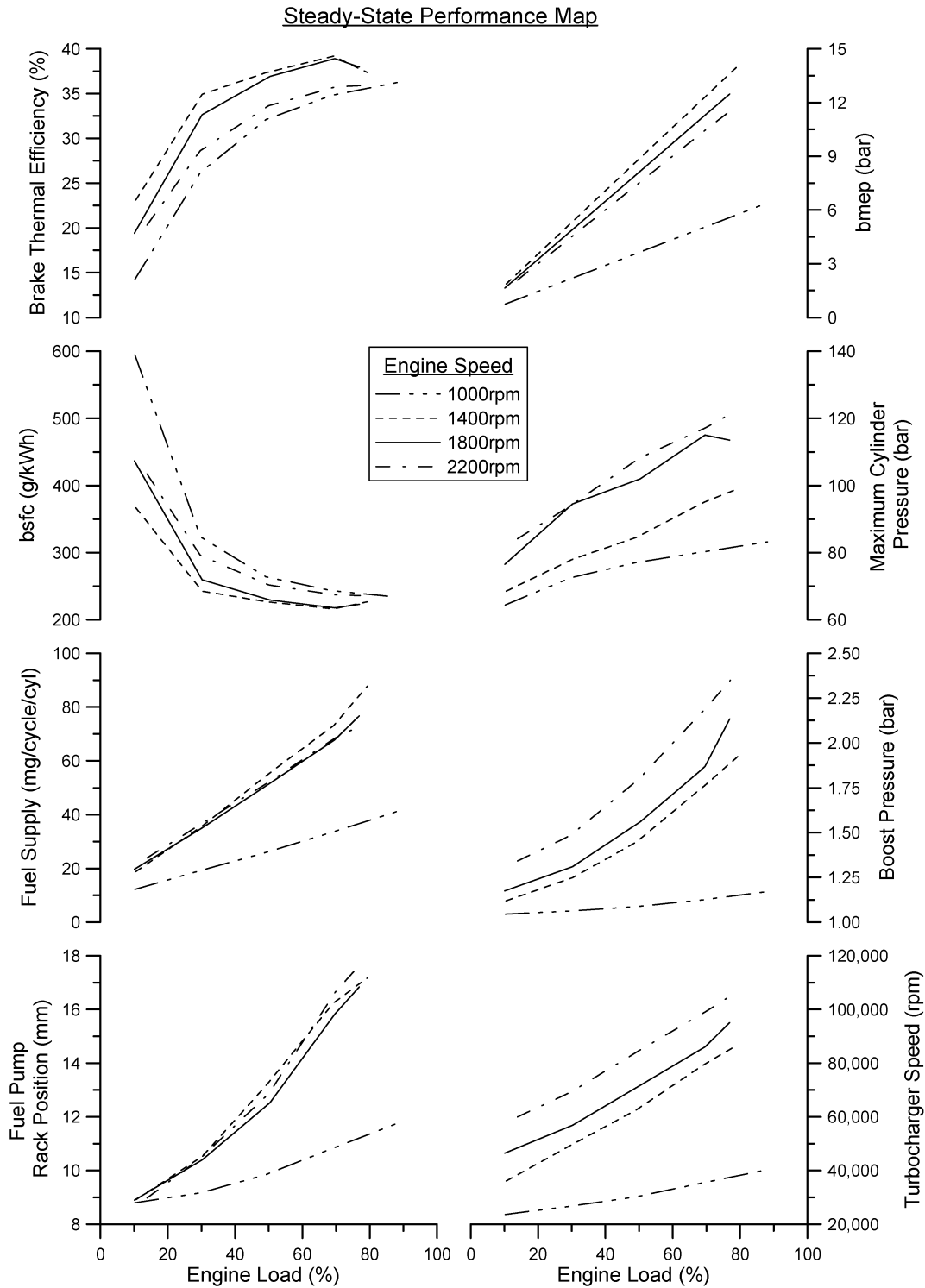


Fig. 3 Steady-state operating parameters and performance map

map of the engine operating parameters and emissions. The *bsfc*, *bmep*, and *bte* were calculated as detailed in section 3.1. At the lowest speed, the engine produces relatively low power and so all operating values are low, except, of course, for *bsfc* that is adversely affected by loading.

As regards the emissions (Fig. 4), the intriguing finding is the high NO values at the 1800 rpm engine speed. A somewhat similar trend can be observed for the combustion noise at the same engine speed; the latter suggests high cylinder pressure gradients resulting from intense premixed combustion, which in turn

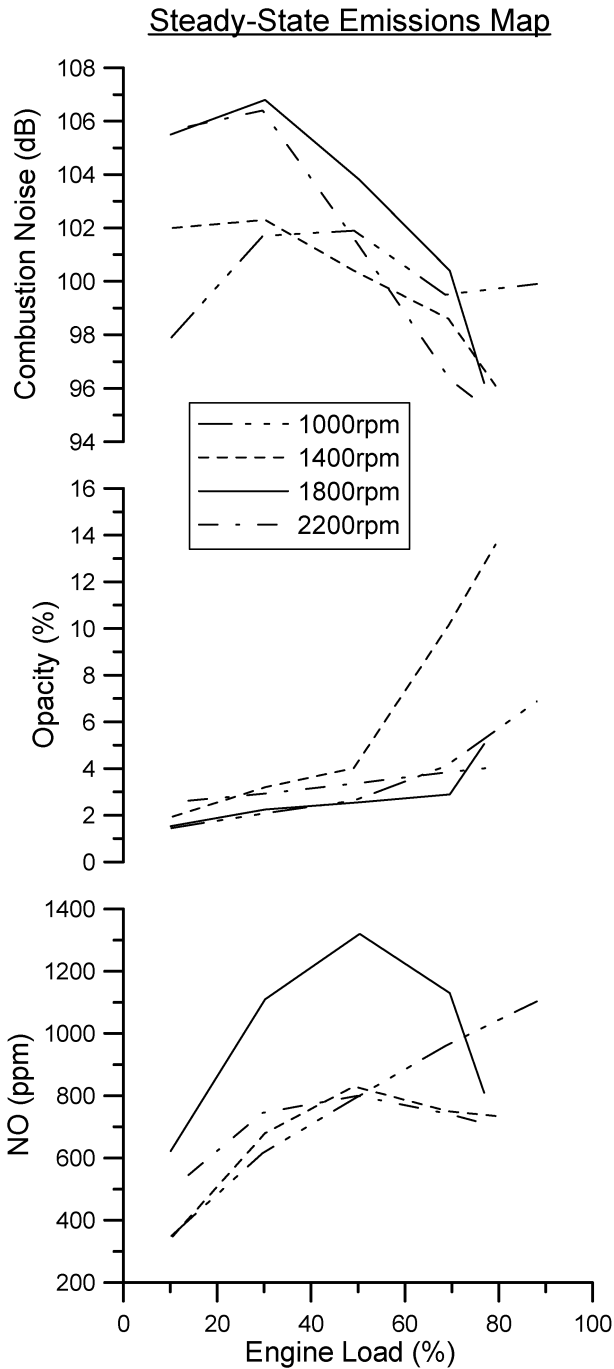


Fig. 4 Steady-state pollutants and combustion noise emissions map

favours NO formation. However, this is only a first qualitative explanation, since there are various parameters that affect the very complex process of NO formation inside the cylinder. For example, the injection timing calibration of the engine plays an important role through its effect on ignition delay, and thus, on premixed combustion phase. From Fig. 4 it can also be observed that for both combustion noise and NO emissions there is a peak observed at roughly

50 per cent engine load for most rotational speeds. This is also attributed to the engine injection calibration, which aims at reducing NO emissions at high loads (see section 2.1 and Table 1). As expected, turbocharger speed and boost pressure develop in a similar manner over the whole engine operating range.

For the smoke emission, it is mainly the loading that plays a significant role. As the load increases, more fuel is injected into the cylinders, increasing the temperature in the fuel-rich zones. Moreover, the duration of diffusion combustion is increased favouring soot formation, whereas the remaining time after combustion as well as the availability of oxygen – both of which enhance the soot oxidation process – decreases; thus, the production of soot (and smoke) is favoured. As will be discussed later, the main mechanism of transient smoke emission is largely based on this key behaviour. As is usually the case with turbocharged diesel engines, high opacity values are noticed for low-speed, high-load engine operation (despite the application of the fuel limiter), due to the limited inlet air supply as the turbocharger compressor produces low boost. This is the case for the 1400 rpm curve in Fig. 4, where smoke opacity peaks at high engine loads.

5.2 Acceleration tests results

5.2.1 Test 1

The results of transient test 1 are presented in Figs 5 and 6. Here, acceleration from an initial engine speed of 1016 rpm and 10 per cent load to a final speed of 1880 rpm and 15 per cent load was conducted in two different modes. The first one was a one-step acceleration, whereas the second one was a multi-step speed increase, with the engine allowed to partly stabilize at two intermediate speeds, i.e. 1491 rpm and 1668 rpm, forming in that way a three-step acceleration. These steps can be identified in the curves of fuel pump rack position and engine speed in Fig. 5. More specifically, the rack position assumes three peak values (in cycles 24, 119, and 159) reaching its final steady-state position after 225 engine cycles (approximately at  $t = 16$  s). On the other hand, during the single-step acceleration, the rack shifts instantly to its maximum fuel supply position after the pedal is pushed and the acceleration concludes much faster (in 'just' 5 s). The direct impact of rack movement on engine speed is illustrated in Fig. 5 too, with the turbocharger speed and boost pressure values affected accordingly.

The development of the maximum cylinder pressure follows closely the rack movement profile, but it

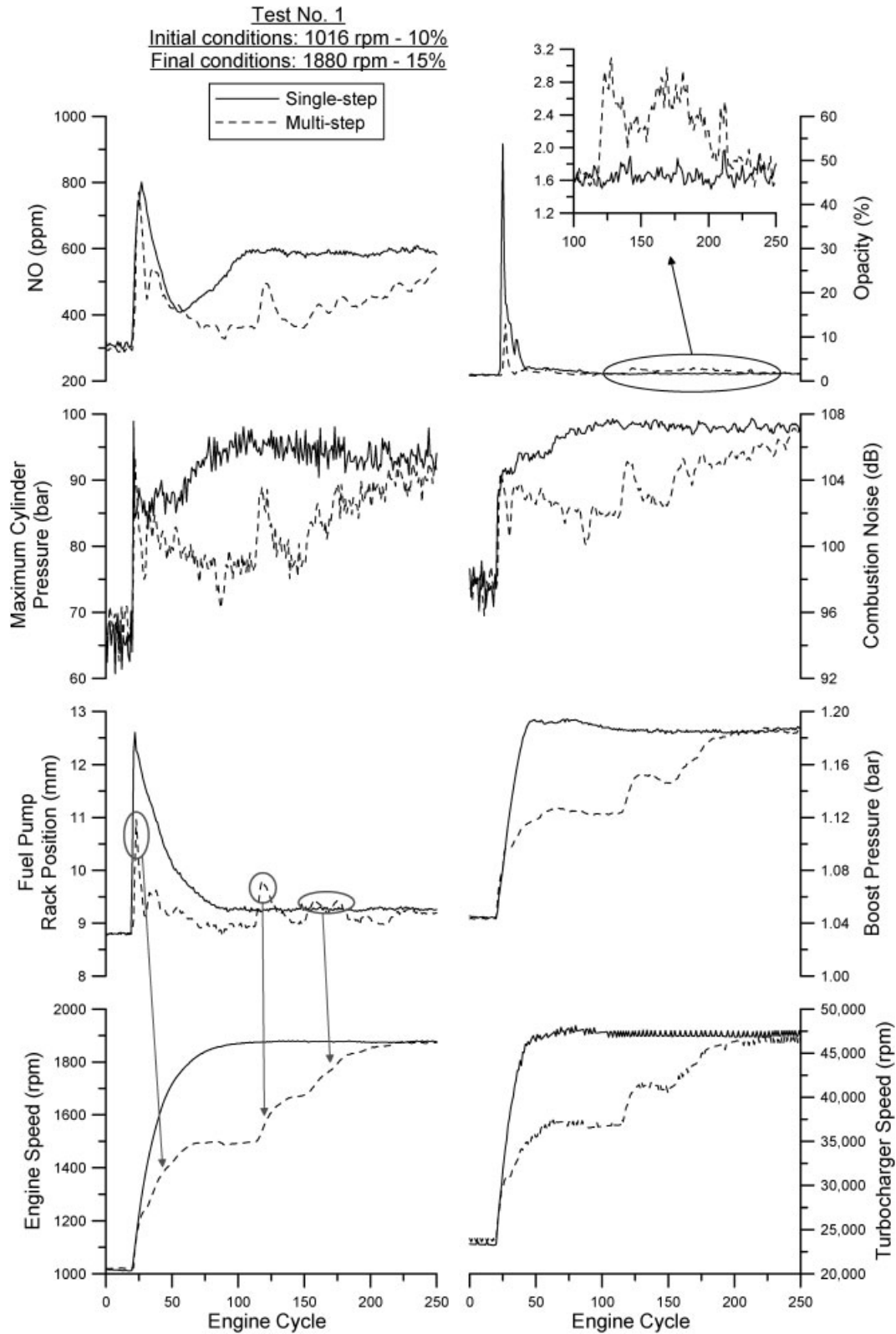


**Fig. 5** Development of engine and turbocharger parameters and emissions response during single-step and multi-step acceleration

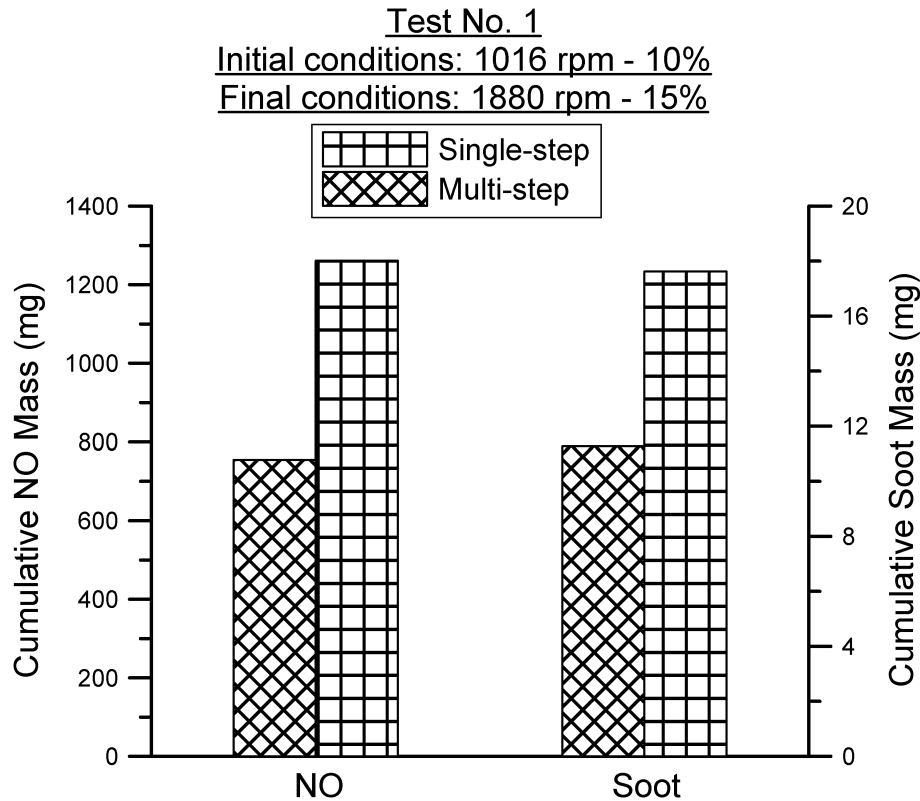


**Fig. 6** Total NO and soot mass emitted during single-step and multi-step acceleration

also incorporates the influence of the relative boost pressure increase and the injection timing change. During the single-step acceleration, maximum cylinder pressure instantaneously assumes a first peak following the shift of the fuel pump rack to its maximum position and then decreases as the rack moves backwards to sustain the achieved engine speed. The subsequent gradual increase of the cylinder pressure (after approximately cycle 50) is attributed to the respective boost pressure development. The same comments apply for every stage of the multi-step acceleration, where the concurrence between maximum cylinder pressure and fuel pump rack movement is evident.

As far as emissions are concerned, major differences are observed between the two studied acceleration cases, with the smoke opacity values presenting the greatest deviations between the two examined transients. Excessive opacity values (Fig. 5 upper right-hand side sub-diagram) are experienced during the single-step acceleration, clearly attributed to the harder turbocharger lag period. The abrupt increase in fuelling combined with the still low (practically unchanged) air supply during the early cycles of this test case result in high values of fuel-air equivalence ratio. Moreover, the very low boost pressure leads to low in-cylinder pressures at the fuel injection timing, resulting

in increased fuel spray penetration, wall impingement, and consequently elevated soot emission. The opacity ultimately stabilizes to its final equilibrium value after the rack has shifted to lower fuellings, and the boost pressure has increased adequately.

During the multi-step acceleration, things run quite smoothly, since each individual step involves acceleration between narrower engine speed limits, hence peak fuellings are lower, and there is sufficient time for boost pressure to develop. Thus, fuel spray penetration and wall impingement are reduced and much lower opacity values are observed (up to four times lower compared with the values during the single-step acceleration). It is interesting to note that instantaneous soot emission spikes, although of much lower magnitude, do occur during the second and third step of this acceleration between the 100<sup>th</sup> and the 200<sup>th</sup> cycle ('zoomed' in the small figure in the opacity sub-diagram).

As is expected, cumulative soot mass is higher during the single-step acceleration compared to the multi-step case. The difference, illustrated in Fig. 6, is of the order of 56 per cent. For the values shown in Fig. 6, opacity has been converted into mass per engine cycle following the procedure described in section 3.3, and the summation is executed until the multi-step case equilibrates.

NO emission is also strongly influenced by the lag between increased fuelling and the response of the air-charging system discussed earlier, resulting in increased emissions as shown in Fig. 5. Since the main parameter affecting NO formation is the burned gas temperature, local high temperatures due to close to stoichiometric fuel-air mixtures (formed because of the still low air-supply) are expected to increase NO during the turbocharger lag cycles. The well known dependence of NO formation on gas temperature can be documented in Fig. 5 by the similarity in the development histories between NO and maximum cylinder pressure in both acceleration cases. In particular during the multi-step acceleration, many local NO peaks occur before the final stabilization is achieved. These peaks are directly related to the respective peaks of maximum cylinder pressure (Fig. 5), which in turn are reflected in gas temperature peaks. The synergistic effect of greater spikes and faster recovery period during the single-step acceleration produces elevated cumulative NO mass (Fig. 6), with the difference reaching 67 per cent compared with the multi-step transient.

The last class of emission studied here is combustion noise, which is closely related to cylinder pressure [34]. In fact, its measuring principle is based on the processing of the measured indicator diagrams. In both test cases illustrated in Fig. 5, combustion noise emission seems to develop in accordance with the maximum cylinder pressure profile. Especially during the multi-step case, combustion noise seems to follow every maximum cylinder pressure local peak as well as its overall trend. However, this is not exactly the case, since combustion noise is influenced primarily by the rate of cylinder pressure increase (i.e. its gradient with respect to crank angle/time) during the engine cycle [35, 36]. This rate is affected by a variety of parameters, including injection timing and ignition delay. During acceleration (or load increase) both parameters behave differently compared with the respective steady-state conditions (especially for the turbocharger lag cycles).

### 5.2.2 Test 2

An important parameter that significantly affects engine and turbocharger response as well as emissions development during acceleration is the rate of the (accelerator) pedal movement from the initial to its final position. In real-world driving, this represents the aggressiveness of the driver. Its impact on engine performance and emissions is studied in Figs 7 and 8. Here, an acceleration test from 1420 to 1845 rpm was performed twice, once in 'fast' and the second in 'slow' mode. The time needed for the fuel pump rack

to shift to its maximum position can be used as an index of the time over which the pedal position change took place. This period was 1 s for the 'fast' and 5 s for the 'slow' mode.

From Fig. 7 it is obvious that the difference in the acceleration rate can be quite dramatic and the qualitative remarks that follow may be applicable on a general basis. The repeatability of the test was ensured by the adjustable custom made 'stop', which was fitted on the pedal (described in section 2.3). This is also confirmed by the initial and final values of all engine and turbocharger variables being practically the same for both acceleration modes. Thus, the only parameter affected by the rate of the pedal movement is the development profile of the measured variables, as has been previously reported in the literature [3, 37].

As illustrated in Fig. 7, the most important difference between the two acceleration modes is observed in the fuel pump rack position development. In the case of the rapid pedal push, the rack is forced to travel almost instantaneously to its maximum position before gradually settling down to its final steady-state value, corresponding to the desired engine speed. However, the fuel pump rack responds in two stages; initially a rapid shift to a first peak position is observed, followed by a smoother movement to the maximum position. The latter behaviour highlights, in the most explicit way, the fuel limiter operating principle that does not allow sharp fuelling increases when the boost pressure is still low. On the contrary, when the pedal is pushed slowly ('slow' transient), the rack shifts at a much smoother rate (no fuel limiter action needed here), causing lower acceleration rates and slowing down the whole transient event. As a result, all the other interesting operating parameters (most significantly pollutant and noise emissions) also develop in a smoother way.

It is the opacity that assumes considerably higher peak values during the 'fast' acceleration test. The difference in maximum opacity values for the specific test is up to 60 per cent between the two acceleration modes. This is attributed to the greater impact the turbocharger lag effect has, the faster the application of the new fuelling is. During the fast acceleration, boost pressure builds-up slowly causing a worse mismatch with fuelling. Thus, even more fuel is injected into a, practically, unchanged air-environment, resulting in greater fuel spray penetration and wall impingement. The heterogeneity of the mixture is increased, with more fuel-rich regions forming inside the cylinder and eventually resulting in greater soot emission spikes.

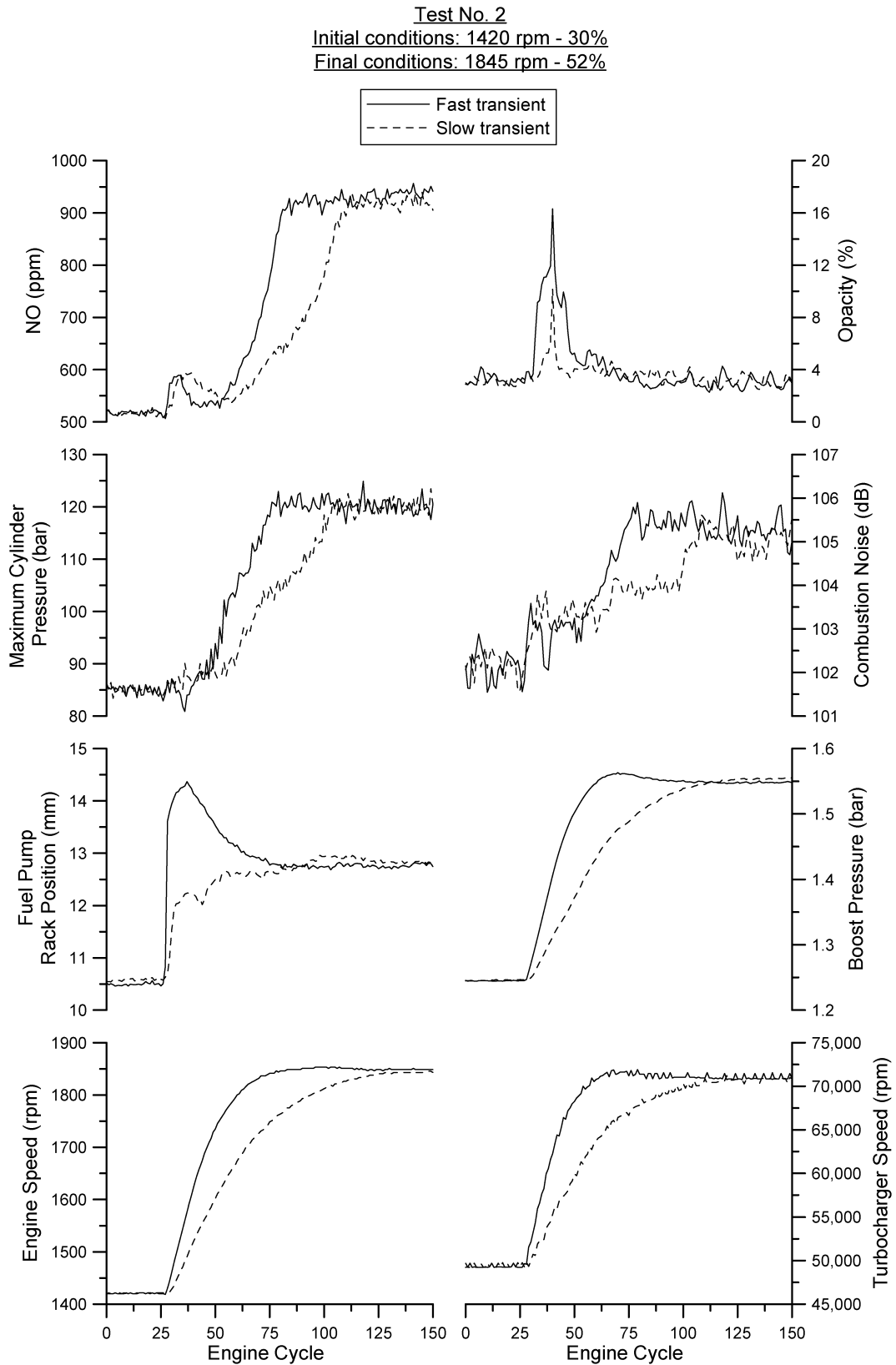
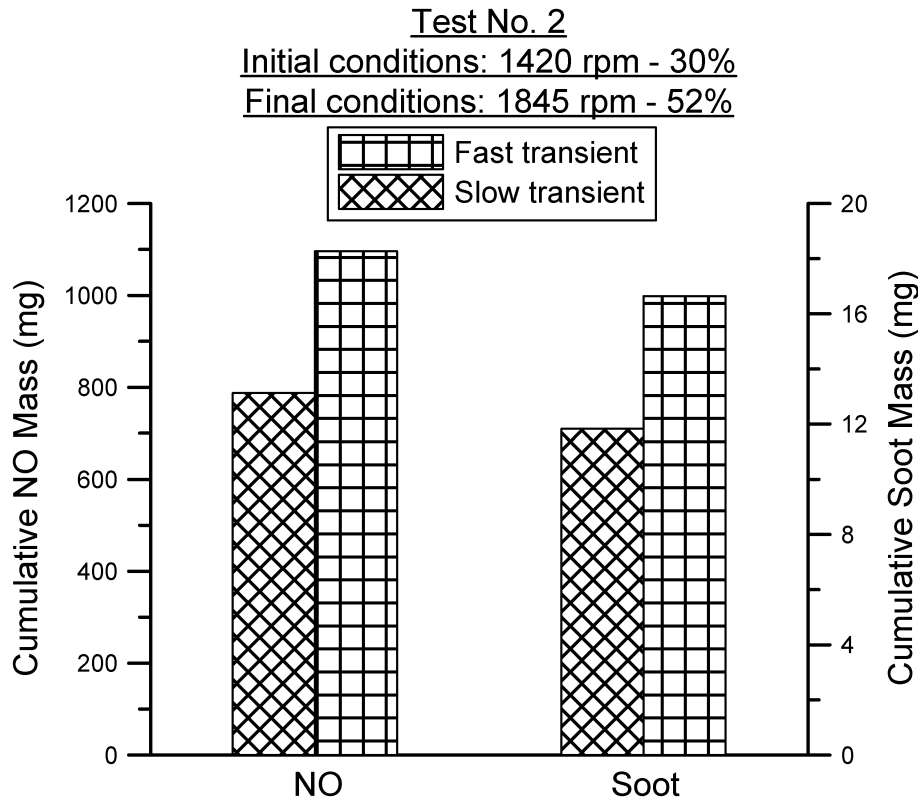


Fig. 7 Development of engine and turbocharger parameters and emissions response during fast and slow acceleration



**Fig. 8** Total NO and soot mass emitted during fast and slow acceleration

The behaviour of the other two emissions, NO and combustion noise, do not seem to be significantly influenced by the rate of speed increase compared to its effect on the opacity. The main difference noticed here is a delay in their development. Again, the NO profile closely follows the maximum cylinder pressure profile (as discussed earlier). During the 'fast' transient, NO reaches its final steady-state value faster compared with the 'slow' transient but the higher peak values result also in greater cumulative NO mass emitted. Similar remarks hold for the combustion noise radiation, which needs even more engine cycles to reach its final steady-state value during the 'slow' acceleration case.

Cumulative NO and soot mass values for acceleration test 2 are presented in Fig. 8. It should be noted that the summation of NO and soot mass for the calculation of their cumulative values during the transient event is performed until the point where final equilibrium has been reached for the 'slow' case. A longer period with high opacity values (also with greater spikes as depicted in Fig. 7) is the main reason for higher total mass values for soot and NO during the 'fast' acceleration case. The difference in cumulative mass between the two acceleration modes studied here is 39 per cent for NO and 41 per cent for soot.

### 5.2.3 Test 3

During daily driving, automotive diesel engines experience quite a few 'combined' transient schedules. A typical case is when a vehicle starts climbing a hill (load increase) and the driver shifts to a lower gear and pushes the pedal in order to accelerate the engine, which in turn offers higher torque to the driving wheels to overcome the increased resistance. Such a transient schedule is studied in test 3, characterized by a simultaneous load (resistance) and speed increase. The conditions at each stage of this test are given in Table 5. The development of various operating parameters and emissions during this test is presented in Fig. 9.

During the first part of this test, a (rather slow) movement of the brake control lever was initiated towards the direction of increased loading (load increase) without change of the engine accelerator pedal position. It should be noted here that while automotive engines do encounter load increase transients they are not as pronounced as the ones experienced by industrial or marine engines. The most significant factor that determines the engine response after a load increase is the governor operating curves [2]. For the specific case used in this test, the application of the new higher load caused a decrease in engine speed of about 300 rpm, which influenced the whole system response during the first part of the test. It is worth mentioning that due

**Table 5** Conditions at each part of the combined test 3

	Speed (rpm)	Load (%)
Initial conditions	1825	30
Test 3 – Part I: Load increase Intermediate conditions	1530	42
Test 3 – Part II: Acceleration Final conditions	2022	77

to the less tight governing of automotive engines compared to industrial ones, severe load changes on an uncontrolled automotive test bench may lead to engine stall.

During the application of the new higher load ('Part I'), the governor shifts the rack to greater fuel delivery positions in response to the instantaneous speed drop. However, based on the specific governor operating curves, the engine speed decreases quickly, which (combined with the increased fuelling) results in a moderate only increase in the turbocharger speed and boost pressure. After the engine has stabilized to a lower speed/higher load condition, the pedal is pushed ('Part II') to accelerate the engine to a higher speed; at the same time, load increases too since the hydraulic dynamometer's torque roughly depends on the square of its rotational speed (the same trend applies also to vehicular aerodynamic resistance). The rack is forced to shift to much greater fuelling positions, while turbocharger speed and boost pressure increase sharply.

For NO emission during this 'combined' transient test, a slightly increasing trend is initially observed owing to the increased fuelling resulting from the governor response as the engine speed drops. However, the large speed drop experienced at this stage is dominant, causing a decrease of in-cylinder pressures (as shown in the maximum cylinder pressure sub-diagram in Fig. 9), which in turn are translated into lower gas temperatures, thus lower NO formation. The subsequent acceleration ('Part II') causes a sharp increase in NO emission as already discussed in the previous sections.

As far as combustion noise is concerned, a general decreasing trend is noticed throughout the whole test, with local spikes experienced only at the start of the acceleration. This behaviour is closely related to the development of the respective cylinder pressure gradient, illustrated in Fig. 10, and is due to the specific engine injection calibration (late injection timing to control NO emissions at medium-high loads). It is interesting again to observe the qualitative correlation between combustion noise development and NO emission response; during 'Part I', both of them exhibit an initial decrease with a subsequent increase during 'Part II' of the test.

Finally, exhaust gas opacity develops in a slow manner during the load increase ('Part I') owing to the moderate change of fuel pump rack position (as determined by the governor operating curves). In contrast, at the initiation of acceleration ('Part II'), opacity reaches a peak value with subsequent local spikes following the fuel pump rack position response. Clearly, the turbocharger lag effect is much more prominent during the acceleration part of this 'combined' transient test, where the instantaneous high fuelling at the beginning of the acceleration is not accompanied by sufficient increase of the air supply (owing to the slowly developing boost pressure), resulting in the previously mentioned opacity peaks.

## 6 QUASI-STEADY APPROXIMATION

In order to shed more light into the impact of transient conditions on pollutants and combustion noise emissions, a quasi-steady prediction of the emissions was undertaken (for the instantaneous rotational speed and fuel pump rack position of each cycle during the transient event). It should be noted that such approximate techniques are sometimes used for transient performance and emissions prediction purposes, applying additional correction coefficients to the steady-state values to account for transient discrepancies [21, 22]. Alternatively, a quasi-steady-state engine characterization methodology has been proposed that aims at estimating indirectly NO and soot emissions for a specific transient event [38]. However, in this case the goal was mainly to highlight the different evolution pattern of transient emissions compared with their steady-state counterparts.

The general application procedure of this technique is illustrated in the flowchart of Fig. 11. Initially, steady-state maps of all interesting engine operating parameters and emissions were constructed with respect to engine speed and fuel pump rack position, based on the detailed steady-state measurements discussed in section 5 (in Fig. 11 boost pressure and opacity maps are only presented, as an example). Afterwards, the time (or engine cycle) histories of engine speed and fuel pump rack position were fed as inputs to the look-up tables, generating the quasi-steady values of emissions and performance parameters. This means that the quasi-steady approximation provides an estimation of emissions values if the engine was allowed to stabilize at each intermediate point of the transient event.

A typical example of quasi-steady approximation and its deviation from 'real' transient data is illustrated in Fig. 12. Here, test 4 (Table 2) is studied on a quasi-

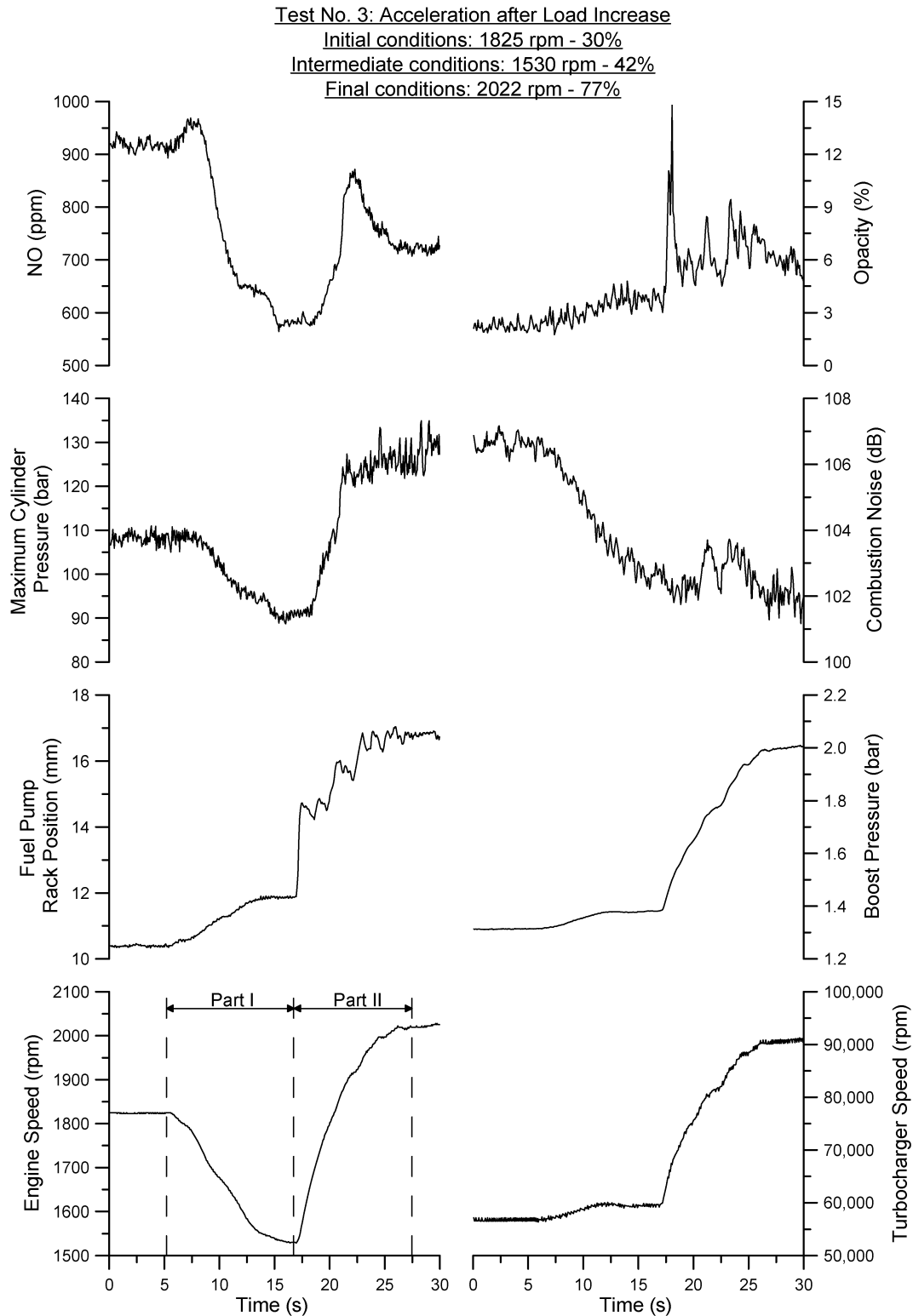


**Fig. 9** Development of engine and turbocharger parameters and emissions response during acceleration after load increase (gear shift)

steady basis and compared with the experimental transient measurements. The development profiles of boost pressure, soot, NO, and combustion noise emissions are presented, together with the engine speed, rack

position, and maximum cylinder pressure responses. The major observations concern on the one hand the absolute values of (peak) emissions, and on the other hand the timing at which these occur.

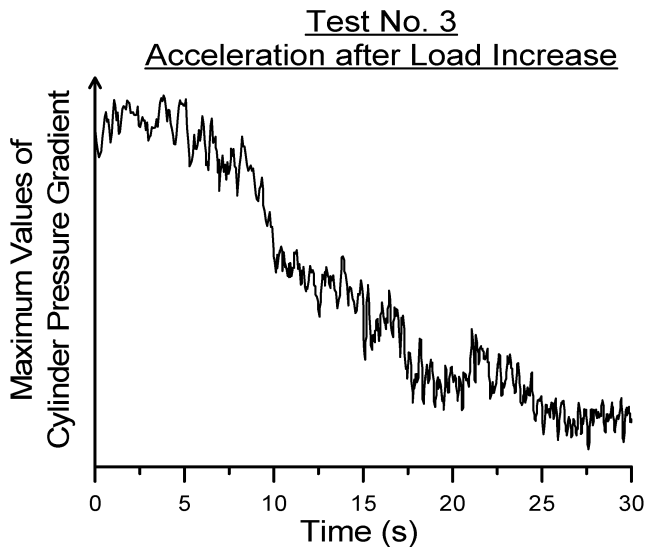


**Fig. 10** Development of maximum cylinder pressure gradient (rate of cylinder pressure increase) with respect to crank angle for test 3

It is the opacity values that highlight in the most explicit way the different evolution profile between real (transient) and quasi-steady development. As is apparent from Fig. 12, transient soot assumes dramatically higher peak values than its quasi-steady counterpart. For the specific test case, this difference reaches up to 4.4 times the quasi-steady peak value, with even higher discrepancies experienced for other 'harder' acceleration cases. On the other hand, transient peak soot exhibits a small delay of about four engine cycles compared with the quasi-steady values; this is primarily attributed to the distance the gas has to travel until it reaches the measuring location.

The three basic reasons that explain the serious discrepancy between quasi-steady and experimental transient opacity values can be described as follows.

1. The air mass flowrate develops during the transient event at a much different (slower) rate owing to turbocharger lag (the greater the differences the higher the acceleration or the faster the accelerator pedal change); the boost pressure development in Fig. 12 clearly highlights this behaviour.
2. Fuel delivery to the cylinders is also differentiated, owing to the injection timing alteration during transients; the developing value of residual pressure in the fuel injection line [2] and the instantaneous torsional deformations in the driving system of the (mechanical) fuel injection pump [39] cause rapid and considerable changes to the dynamic injection and fuelling.
3. Cylinder wall temperature develops more slowly during acceleration, owing to the thermal inertia

of the cylinder-wall-coolant system. Lubrication oil temperature, which also plays an important role through its impact on engine friction, develops more slowly during transients compared with steady-state conditions [4].

As far as NO emission is concerned, the trend is, however, different. Quasi-steady peak values were actually found to be higher than their transient counterparts, with the same remark also applying to the final values. The difference in the maximum values may be caused by the injection timing alteration discussed previously, the complete worsening of fuel-air mixing (for example, oxygen shortage is experienced due to low boost pressures during the turbocharger lag cycles diminishing the transient NO production rate), as well as by the slowly developing thermal transient, which leads to higher thermal losses to the cylinder walls and decreases the gas temperature. The latter is also responsible for the difference observed between the final quasi-steady and transient values. Again, the delay in the peak values between the real transient measurement and the quasi-steady approximation is attributed both to the completely different operating conditions, as well as to the distance the gas has to travel until it reaches the measuring location.

Another notable effect that significantly affects both smoke and NO emissions during transient operation is the *internal* exhaust gas recirculation. During the first cycles of the transient event, the boost pressure remains practically unchanged or develops in a very slow rate, while (maximum) cylinder pressure rises quickly (due to greater fuel mass injected), as shown in Fig. 12. As a result, the engine exhaust back pressure increases (i.e. the ratio of back to boost pressure is higher), thus the exhaust gas backflow during the valve overlap period is more intense and the amount of residual gas in the cylinder becomes larger [40] compared with its steady-state counterpart. This results in lower NO values, due to the thermal effect of residual gas, which limits maximum combustion temperature (and thus NO); however, higher soot values are experienced since the above phenomenon causes a further decrease in the air-fuel ratio (i.e. more fuel-rich regions in the cylinder), as the residual gas replaces oxygen [2, 41].

Finally, combustion noise radiation is higher during the transient event (especially during the turbocharger lag cycles) compared with the quasi-steady operation, confirming the results of previous research [26]. The main mechanism behind the increase in combustion noise radiation during transients lies in the operating principles of a transient event. During the first cycles after a speed (or load) increase, the injected fuel quantity has already increased substan-

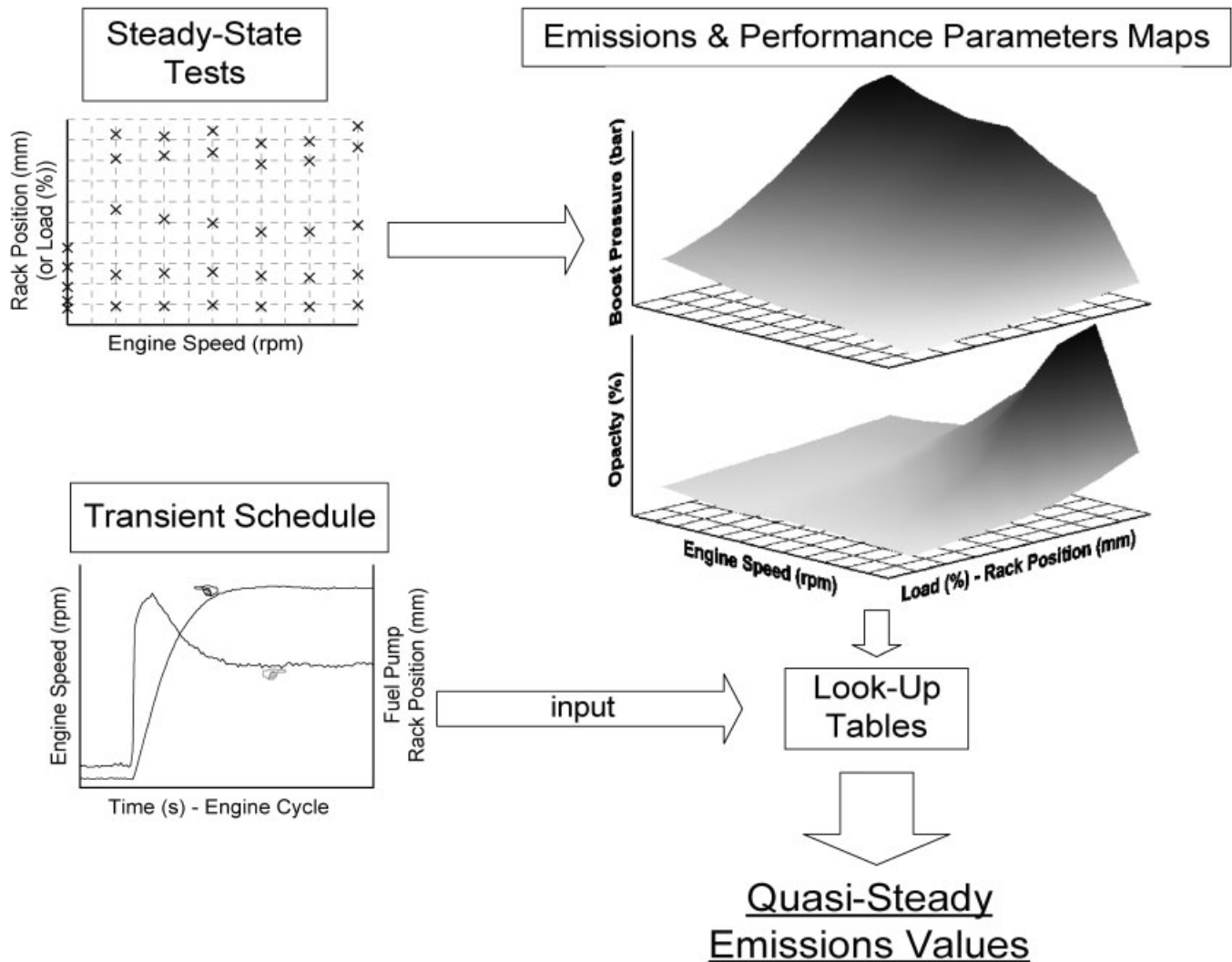


Fig. 11 Flowchart showing the methodology for the quasi-steady approximation of emissions

tially cooling down the charge-air temperature; however, the cylinder wall temperature is still low (up to 100 °C lower than the corresponding steady-state conditions) as the thermal transient proceeds at a much slower rate due to the cylinder wall thermal inertia [42]. The combination of increased fuelling with the still low cylinder wall temperature and ‘cooled’ charge-air temperature results in longer ignition delay, hence more intense premixed combustion periods leading to steeper cylinder pressure gradients and, consequently, higher combustion noise levels [2, 26].

The arguments introduced previously highlight, on the one hand, the importance of transient operation study and, on the other hand, its complexity and its completely different evolution pattern compared with steady-state operation, requiring careful and systematic experimental and simulation analysis. Clearly, transient turbocharged diesel engine operation cannot be considered as a series of steady-state operating

points, nor can the engine be assumed to behave in a quasi-steady manner during transients.

## 7 CONCLUSIONS

A fully instrumented test bed installation has been developed in order to study the transient performance and emissions of an automotive/truck turbocharged diesel engine. Fast response analysers were employed for measuring NO, smoke opacity, and combustion noise emissions for a variety of acceleration tests experienced during daily driving conditions. Furthermore, a quasi-steady approximation was undertaken in order to highlight the completely different evolution pattern of transient conditions compared with steady-state operation. The basic conclusions derived from the current investigation, for the specific engine-hydraulic-brake configuration, can be summarized as follows.

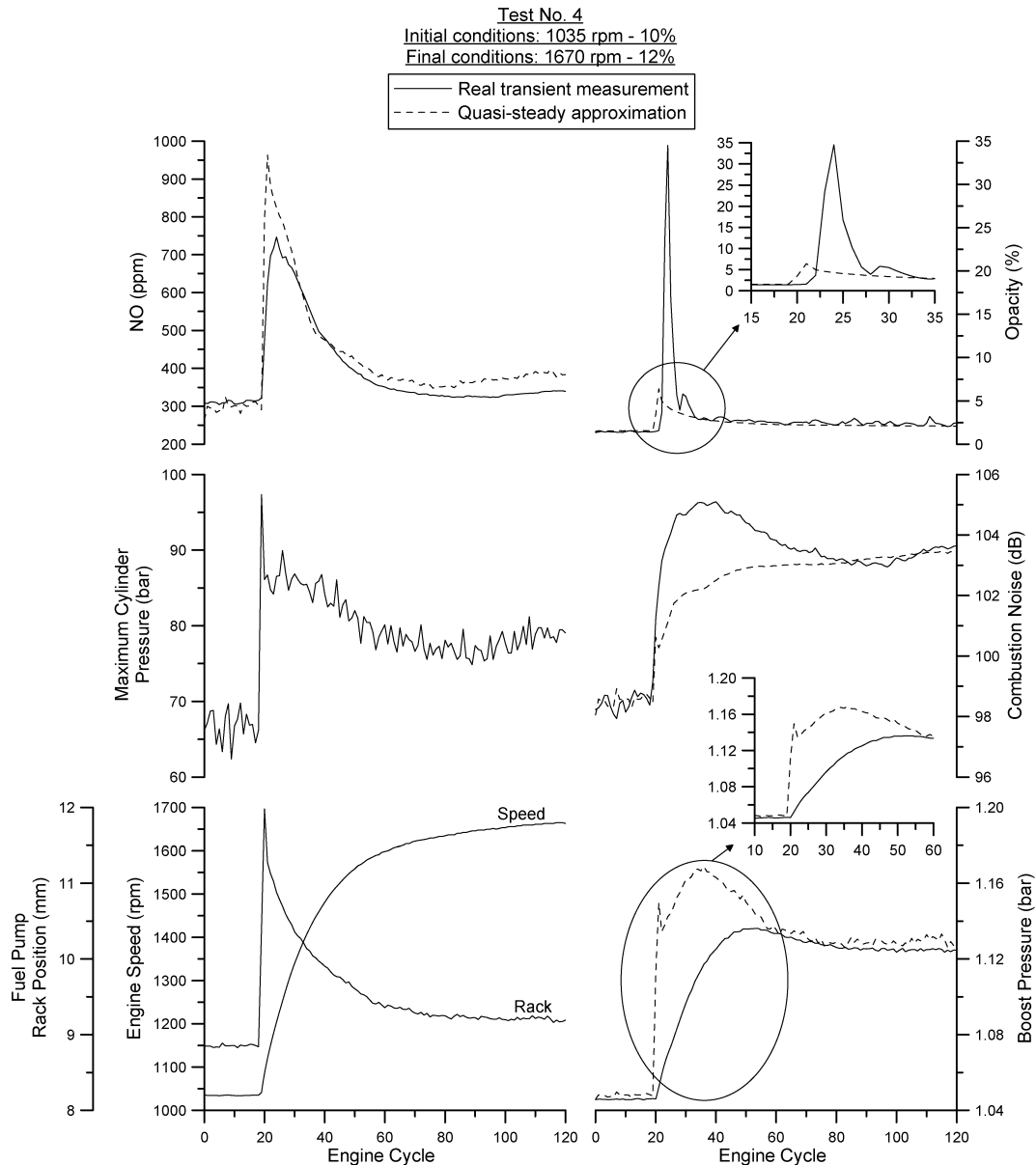


**Fig. 12** Quasi-steady approximation of emissions during acceleration test 4 (Table 2) and comparison with actual transient measurements

- As expected, turbocharger lag was found to be the most notable contributor for all the examined transient test cases, and the major cause for high values of NO, smoke, and combustion noise emissions.
- Fuel limiter action, governing, turbocharger characteristics, engine injection timing calibration, and individual specifications of each test were found to strongly affect the speed response as well as the profile and cumulative values of all pollutants.
- Combustion noise is directly influenced by the in-cylinder pressure gradient, and may be affected by the specific engine calibration (for the particular engine this consists of retarded injection timing for the purpose of NO emission limitation).
- Turbocharger lag effects were much less prominent during multi-step, or slow acceleration, resulting in much lower opacity spikes. NO and combustion noise emissions are also lower during such transients.
- The rate of the accelerator pedal 'push' affected only the development profile of all operating parameters and emissions, with the final steady-state values being the same in both 'fast' and 'slow' modes. Also, a considerable difference in cumulative NO and soot mass was observed.
- Load increases of an automotive engine on an uncontrolled test bench are strongly influenced by the 'loose' governing, leading to considerable speed

drops and so affecting accordingly the whole system response and emissions development.

7. Transient emissions develop in a completely different manner compared with their steady-state counterparts, owing to the off-design phenomena experienced during dynamic engine operation.

It is believed that the present study has contributed towards a deeper understanding of the complex phenomena experienced during diesel engine transient operation, particularly as regards NO, smoke, and combustion noise emissions development. It can form a basis for deeper research in this challenging field, extending into the investigation of complex transient events and legislated Transient Cycles.

#### ACKNOWLEDGEMENTS

The authors would like to thank Cambustion Ltd (Cambridge, UK) for the loan of the CLD500 NO analyser and, particularly, Dr M. Peckham for his continuous support during the experimental investigation of the engine. Special thanks are due to Turbo Hellas Trading Ltd for the donation of the turbocharger speed sensor kit used in the experiments.

© Authors 2011

#### REFERENCES

- 1 European Automobile Manufacturers' Association (ACEA), available from <http://www.acea.be> (accessed 20 December 2009).
- 2 **Rakopoulos, C. D.** and **Giakoumis, E. G.** *Diesel engine transient operation*, 2009 (Springer, London, UK).
- 3 **Hagena, J. R., Filipi, Z. S., and Assanis, D. N.** Transient diesel emissions: analysis of engine operation during a tip-in. SAE paper 2006-01-1151, 2006.
- 4 **Rakopoulos, C. D.** and **Giakoumis, E. G.** Review of thermodynamic diesel engine simulations under transient operating conditions. SAE paper 2006-01-0884, 2006.
- 5 **Gullett, B. K., Touati, A., Oudejans, L., and Ryan, S. P.** Real-time emissions characterisation of organic air toxic pollutants during steady-state and transient operation of a medium duty diesel engine. *Atmos. Environ.*, 2006, **40**, 4037–4047.
- 6 **Wijetunge, R. S., Brace, C. J., Hawley, J. G., Vaughan, N. D., Horrocks, R. W., and Bird, G. L.** Dynamic behaviour of a high speed direct injection diesel engine. SAE paper 1999-01-0829, 1999.
- 7 Automotive section: directives and regulations on motor vehicles, available from <http://ec.europa.eu/enterprise/sectors/automotive/documents/directives/motor-vehicles/> (accessed 20 December 2009).
- 8 European transient cycle (ETC), available from <http://www.dieselnet.com/standards/cycles/etc.html> (accessed 20 December 2009).
- 9 Dynamometer driver's aid, available from <http://www.epa.gov/nvfel/testing/dynamometer.htm#engcycles> (accessed 20 December 2009).
- 10 **Korakianitis, T., Papagiannidis, P., and Vlachopoulos, N. E.** Unsteady flow/quasi-steady heat transfer computations on a turbine rotor and comparison with experiments. *Trans. ASME, J. Turbo-machinery*, 2002, **124**, 152–159.
- 11 **Korakianitis, T., Vlachopoulos, N. E., and Zou, D.** Models for the prediction of transients in closed regenerative gas turbine cycles with centrifugal impellers. *Trans. ASME, J. Engineering for Gas Turbines and Power*, 2005, **127**, 505–513.
- 12 **Kang, H.** and **Farell, P. V.** Experimental investigation of transient emissions (HC and NO<sub>x</sub>) in a high speed direct injection (HSDI) diesel engine. SAE paper 2005-01-3883, 2005.
- 13 **Black, J., Eastwood, P. G., Tufail, K., Winstanley, T., Hardalupas, Y., and Taylor, A. M. K. P.** Diesel engine transient control and emissions response during a European extra-urban drive cycle (EUDC). SAE paper 2007-01-1938, 2007.
- 14 **Campbell, B., Peckham, M., Symonds, J., Parkinson, J., and Finch, A.** Transient gaseous and particulate emissions measurements on a diesel passenger car including a DPF regeneration event. SAE paper 2006-01-1079, 2006.
- 15 **Armas, O., Cardenas, M. D., and Mata, C.** Smoke opacity and NO<sub>x</sub> emissions from a bioethanol-diesel blend during engine transient operation. SAE paper 2007-24-0131, 2007.
- 16 **Rakopoulos, C. D., Dimaratos, A. M., Giakoumis, E. G., and Peckham, M. S.** Experimental assessment of turbocharged diesel engine transient emissions during acceleration, load change and starting. SAE paper 2010-01-1287, 2010.
- 17 **Cui, Y., Deng, K., and Wu, J.** A modelling and experimental study of transient NO<sub>x</sub> emissions in turbocharged direct injection diesel engines. *Proc. IMechE, Part D: J. Automobile Engineering*, 2004, **218**(5), 535–541. DOI: 10.1243/095440704774061183.
- 18 **Bazari, Z.** Diesel exhaust emissions prediction under transient operating conditions. SAE paper 940666, 1994.
- 19 **Chan, S. H., He, Y., and Sun, J. H.** Prediction of transient nitric oxides in diesel exhaust. *Proc. IMechE, Part D: J. Automobile Engineering*, 1999, **213**(4), 327–339. DOI: 10.1243/0954407991526892.
- 20 **Rakopoulos, C. D., Dimaratos, A. M., Giakoumis, E. G., and Rakopoulos, D. C.** Exhaust emissions estimation during transient turbocharged diesel engine operation using a two-zone combustion model. *Int. J. Veh. Des.*, 2009, **49**, 125–149.
- 21 **Ericson, C., Westerberg, B., and Egnell, R.** Transient emission predictions with quasi stationary models. SAE paper 2005-01-3852, 2005.
- 22 **Giakoumis, E. G.** and **Alafouzou, A. I.** Study of diesel engine performance and emissions during a

- transient cycle applying an engine mapping-based methodology. *Appl. Energy*, 2010, **87**, 1358–1365.
- 23 **Hauberger, S., Ivanisin, M., and Riemersma, I. J.** Modelling of transient influences on HDV emissions. SAE paper 2001-24-0076, 2001.
- 24 **Beaumont, A. J., Noble, A. D., and Pilley, A. D.** Signal reconstruction techniques for improved measurement of transient emissions. SAE paper 900233, 1990.
- 25 **Chan, S. H., Chen, X. S., and Arcoumanis, C.** Measurement and signal reconstruction of transient nitric oxide emissions in the exhaust of a turbocharged diesel engine. *Trans. ASME, J. Dynamic Systems, Measurement and Control*, 1997, **119**, 620–630.
- 26 **Dhaenens, M., van der Linden, G., Nehl, J., and Thiele, R.** Analysis of transient noise behaviour of a truck diesel engine. SAE paper 2001-01-1566, 2001.
- 27 Commission Directive 96/20/EC of 27 March 1996 adapting to technical progress Council Directive 70/15/EEC relating to the permissible sound level and the exhaust system of motor vehicles, Official Journal L 092, April 1996.
- 28 **Torregrosa, A. J., Broatch, A., Martín, J., and Monelletta, L.** Combustion noise level assessment in direct injection diesel engines by means of in-cylinder pressure components. *Meas. Sci. Technol.*, 2007, **18**, 2131–2142.
- 29 Cambustion Ltd, available from <http://www.cambustion.co.uk> (accessed 10 January 2010).
- 30 CLD500 Fast NO<sub>x</sub> Measurement System, User Manual (version 2.2), Cambustion Ltd., 2008.
- 31 AVL 439 Opacimeter, Operating Manual, AVL, November 2006.
- 32 AVL 450 Combustion Noise Meter. Operating Manual, AVL, August 2000.
- 33 DieselNet Technical Data Sheets, Smoke Opacity Paper, available from <http://www.dieselnets.com/calculator/smoke1.html> (accessed 10 January 2010).
- 34 **Taylor, C. F.** *The internal combustion engine in theory and practice*, volume 2, 1985 (MIT Press, Cambridge, Massachusetts).
- 35 **Anderton, D.** Relation between combustion system and noise. SAE paper 790270, 1979.
- 36 **Osawa, H. and Nakada, T.** Pseudo cylinder pressure excitation for analysing the noise characteristics of the engine structure. *JSAE Rev.*, 1999, **20**, 67–72.
- 37 **Rakopoulos, C. D., Dimaratos, A. M., Giakoumis, E. G., and Rakopoulos, D. C.** Evaluation of the effect of engine, load and turbocharger parameters on transient emissions of diesel engine. *Energy Convers. Mgmt.*, 2009, **50**, 2381–2393.
- 38 **Eastwood, P. G., Tufail, K., Winstanley, T., Darlington, A., Karagiorgis, S., Hardalupas, Y., and Taylor, A. M. K. P.** Estimation of deviations in NO and soot emissions between steady-state and EUDC transient operation of a common-rail diesel engine. SAE paper 2009-24-0147, 2009.
- 39 **Murayama, T., Miyamoto, N., Tsuda, T., Suzuki, M., and Hasegawa, S.** Combustion behaviours under accelerating operation of an IDI diesel engine. SAE paper 800966, 1980.
- 40 **Filipi, Z., Hagen, J., and Fathy, H.** Investigating the impact of in-vehicle transients on diesel soot emissions. *Thermal Sci.*, 2008, **12**(1), 53–72.
- 41 **Yokomura, H., Kouketsu, S., Kotooka, S., and Akao, Y.** Transient EGR control for a turbocharged heavy duty diesel engine. SAE paper 2004-01-0120, 2004.
- 42 **Rakopoulos, C. D. and Mavropoulos, G. C.** Effects of transient diesel engine operation on its cyclic heat transfer: an experimental assessment. *Proc. IMechE, Part D: J. Automobile Engineering*, 2009, **223**(11), 1373–1394. DOI: 10.1243/09544070JAUTO1223.

## APPENDIX

## Notation

$bmep$	brake mean effective pressure (bar)
$bsfc$	brake specific fuel consumption (g/kWh)
$bte$	brake thermal efficiency
$C$	concentration (ppm)
$D$	cylinder bore (m)
$k$	absorption coefficient ( $m^{-1}$ or $cm^{-1}$ )
$L$	optical path length (m or cm)
$m$	mass (kg or g)
$M_t$	engine brake torque (N m)
$MW$	molecular weight (kg/kmol)
$n$	engine speed (rpm)
$N$	opacity (%)
$p$	pressure ( $N/m^2$ )
$P$	engine brake power (W)
$R_m$	universal gas constant (= 8314.3 J/kmol K)
$s$	piston stroke (m)
$SD$	soot density ( $mg/m^3$ )
$SMC$	soot mass concentration (mg/kg)
$T$	temperature (K)
$V$	volume ( $m^3$ )
$V_{fc}$	volumetric fuel consumption rate ( $m^3/s$ )
$z$	number of engine cylinders
$\Theta$	lower calorific value of fuel (kJ/kg)
$\rho$	density ( $kg/m^3$ )
<i>Subscripts</i>	
eg	exhaust gas
f	fuel
NO	nitric oxide